ACS OMEGA

http://pubs.acs.org/journal/acsodf

Article

# Preferability of Molnupiravir, an Anti-COVID-19 Drug, toward Purine Nucleosides: A Quantum Mechanical Study

Mahmoud A. A. Ibrahim,* Mohammed N. I. Shehata, Nayra A. M. Moussa, Randa R. A. Hemia, Heba S. M. Abd Elhafez, Mohamed K. Abd El-Rahman, Shaban R. M. Sayed, Peter A. Sidhom, Eslam Dabbish, and Tamer Shoeib*

Cite This: *ACS Omega* 2023, 8, 27553−27565

Read Online

ACCESS | Metrics & More | Article Recommendations | Supporting Information

**ABSTRACT:** Structural aspects of molnupiravir complexed with the RNA of the SARS-CoV-2 virus have been recently resolved inside the RNA-dependent RNA polymerase (RdRp), demonstrating the interactions of molnupiravir with purine nucleosides. However, the preference of molnupiravir to interact with one purine nucleoside over another has not been clearly investigated. Herein, the complexation of molnupiravir in its active form with guanosine and adenosine was compared, using sundry density functional theory calculations. The plausible tautomeric structures of the molnupiravir drug in complex with guanosine/adenosine were minutely scrutinized. The relative energy findings outlined the favorability of amino-molnupiravir···keto-amino-guanosine and imino-molnupiravir···amino-adenosine optimized complexes. According to the interaction ($E_{int}$) and binding ($E_{bind}$) energy values, higher preferential base-pairing of molnupiravir with guanosine over the adenosine one was recognized with $E_{int}/E_{bind}$ values of −31.16/−21.81 and −13.93/−12.83 kcal/mol, respectively. This could be interpreted by the presence of three and two hydrogen bonds within the former and latter complexes, respectively. Observable changes in the electronic properties and global indices of reactivity of the studied complexes also confirmed the preferential binding within the studied complexes. The findings from the quantum theory of atoms in molecules and the noncovalent interaction index also support the partially covalent nature of the investigated interactions. For both complexes, changes in thermodynamic parameters outlined the spontaneous, exothermic, and nonrandom states of the inspected interactions. Inspecting the solvent effect on the studied interactions outlined more observable amelioration within the water medium compared with the gas one. These results would be a durable ground for the forthcoming studies concerned with the interactions of the molnupiravir drug with purine nucleosides.

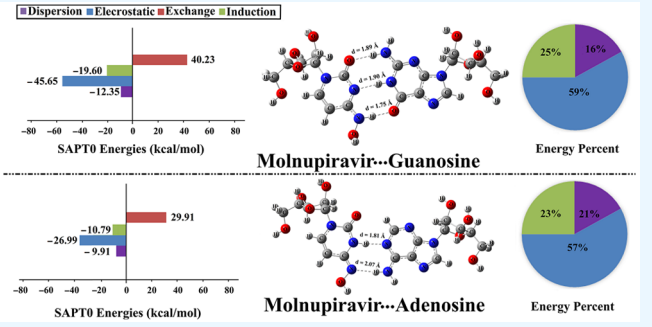


## INTRODUCTION

In December 2019, the novel coronavirus disease (COVID-19) first emerged in Wuhan, China.[1] Owing to its severe symptoms and the catastrophic number of deaths, COVID-19 was declared as a significant public health concern by the World Health Organization (WHO).[2] COVID-19 viral pathogenesis was determined to be triggered via exposure to severe acute respiratory syndrome coronavirus 2 (SARS-CoV-2).[3,4] SARS-CoV-2 is a positive-stranded RNA virus belonging to the betacoronavirus genus.[5,6] Prospective druggable targets in the SARS-CoV-2 virus include the main protease ($M^{pro}$), the papain-like protease ($PL^{pro}$), the spike protein (*S*-protein), and the RNA-dependent RNA polymerase (RdRp). In addition, possible host targets, including the angiotensin-converting enzyme (ACE2) and the transmembrane protease serine 2 (TMPRSS2), are druggable toward COVID-19 treatment.[7,8] Targeting $PL^{pro}$ and 3-chymotrypsin-like protease ($3CL^{pro}$) enzymes would inhibit the reproduction and transcription of SARS-CoV-2.[9,10] The *S*-proteins bind to the ACE2 targets and are a prerequisite for the appearance of COVID-19 infection.[11,12] Alternatively, the TMPRSS2 is included in preparing *S*-proteins, enabling viral entrance into the host cells.[13] The RdRp is in charge of transcription and replication of the viral genome, making it an essential player in the SARS-CoV-2 lifecycle.[14−18]

Structural aspects of RdRp complexed with RNA have recently been released, providing promising mechanistic insights.[15,19] In addition, clarification of the inhibitory mechanism of the RdRp by nucleoside analogues has been demonstrated,[20−22] providing a structural template for developing effective antiviral medications against COVID-19.

**Received:** May 9, 2023
**Accepted:** June 28, 2023
**Published:** July 18, 2023

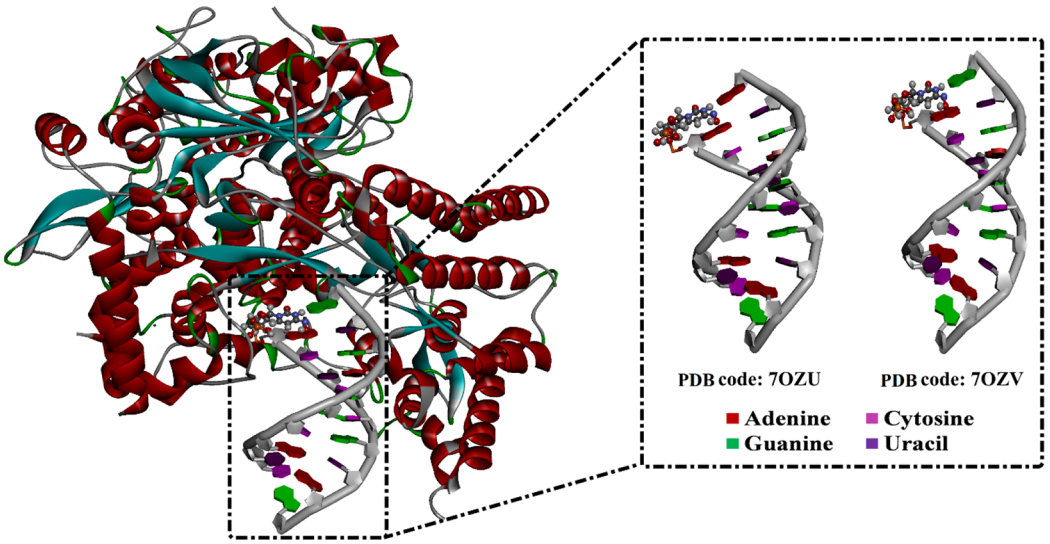


**Figure 1.** Biostructural models of SARS-CoV-2 RdRp with molnupiravir in the template strand base-paired with guanosine (PDB code: 7OZV[27]) and adenosine (PDB code: 7OZU[27]).

Among nucleoside analogues, molnupiravir has recently been authorized for emergency use by the Food and Drug Administration (FDA) for the remediation of COVID-19 infections for both hospitalized and nonhospitalized patients.[23−25] Molnupiravir was first recognized as a promising drug candidate against several viruses, including the respiratory syncytial virus (RSV), the influenza A virus, and the middle east respiratory syndrome coronavirus (MERS-CoV). Detailedly, molnupiravir is an isopropyl ester prodrug of $\beta$-D-$N^4$-hydroxycytidine (NHC) and the first mutagenic nucleoside analogue established to circumvent proofreading.[26]

Principally, the proposed model for the molnupiravir-induced coronavirus RNA mutagenesis mechanism was previously suggested to be accommodated within two steps.[27] The first step involves the synthesis of negative-strand genomic RNA (−gRNA) from the analogue template coined positive-strand genomic RNA (+gRNA). In this step, the diverse tautomeric structures of the molnupiravir drug, especially the amino and imino forms, enable it to be frequently incorporated in the RdRp instead of cytidine and uridine, respectively. Accordingly, the amino and imino forms of the molnupiravir drug behave as pyrimidine nucleosides, and hence, they were allowed for base-pairing, in succession, with the guanine and adenine purine nucleosides, respectively. The second step involves using the resulting molnupiravir-containing RNA for the synthesis of the +gRNA. In turn, the viral propagation is prevented by fostering the error accumulation on the +gRNA (i.e., lethal base-pair mutations) by molnupiravir-containing RNA. Such behavior has been found to be in line with the error catastrophe model.[28−31] Succinctly, the antiviral character of the molnupiravir drug is ascribed to the base-pair mutations.[32]

Exploring the recently resolved structures of molnupiravir complexed with RNA inside the RdRp of SARS-CoV-2 revealed the potential interaction of molnupiravir with guanosine (PDB code: 7OZV) and adenosine (PDB code: 7OZU), as shown in Figure 1.[27] However, the preference of molnupiravir to interact with one purine nucleoside over another has not been clearly investigated.

In this regard, interactions of the molnupiravir in its active form with purine nucleosides were herein fully explored using density functional theory (DFT) computations. Geometrical optimization computations were conducted for the plausible tautomeric structures of the molnupiravir drug in complex with purine nucleosides. Upon the most favorable complexes, frequency calculations were performed, and the interaction ($E_{int}$)/binding ($E_{bind}$) energies were assessed. The physical forces involved in the interactions within the studied complexes were elucidated using the symmetry-adapted perturbation theory (SAPT). Analyses of the quantum theory of atoms in molecules (QTAIM) and noncovalent interaction (NCI) index were subsequently performed. Further assessment of several electronic parameters and global indices of reactivity were established based on data obtained from the frontier molecular orbitals (FMOs) theory. A thorough insight into the thermodynamic features was also established. The solvent effect on the interactions of the molnupiravir drug with the purine nucleosides was also investigated. The obtained findings could find potential use for designing potent nucleoside analogues as inhibitors of viral RNA replication.

## COMPUTATIONAL METHODS

Interactions of molnupiravir in its active form with the purine nucleosides, including guanosine and adenosine, were explored using DFT calculations. Basically, the tautomerization effect on the base-pairing efficiency was carefully scrutinized. First, geometrical optimization computations were performed for the plausible tautomeric structures of the molnupiravir drug in the isolated form and the complexed one with the guanosine/adenosine within the molnupiravir···guanosine/···adenosine complexes using the M06-2X/6-311++G(d,p) level of computation.[33] Afterward, the relative energy ($E_{relative}$) calculations were conducted to determine their relative stability (see eq 1).

$$E_{relative} = E_{tautomer} - E_{tautomer\ in\ the\ most\ stable\ configuration} \quad (1)$$

where $E_{tautomer}$ and $E_{tautomer\ in\ the\ most\ stable\ configuration}$ represent the energy of the tautomer and the energy of the tautomer in the most stable configuration, respectively. Molecular electrostatic potential (MEP) analysis was used to assign the relative electrophilicity and nucleophilicity over the molecular entities of the optimized monomers in forms involved within the


https://doi.org/10.1021/acsomega.3c03215
ACS Omega 2023, 8, 27553−27565

selected complexes. Moreover, the local most positive and most negative electrostatic potential values ($V_{s,max}$ and $V_{s,min}$) were computed. MEP maps along with the $V_{s,max}$ and $V_{s,min}$ values were subsequently generated using electron density envelopes of 0.002 au.[34]

For the molnupiravir complexes with guanosine and adenosine, the initial structures were truncated from their respective PDB codes 7OZV[27] and 7OZU[27] (see Figure 1). Upon the most proficient complexes, frequency computations were carried out at the same level of theory. The interaction ($E_{int}$) and binding ($E_{bind}$) energies were then evaluated considering the counterpoise corrections to eliminate the basis set superposition error (BSSE),[35] via eqs 2 and 3, respectively.

$$E_{int} = E_{\text{Molnupiravir}\cdots\text{Guanosine/Adenosine}} - (E_{\text{Molnupiravir in complex}} + E_{\text{Guanosine/Adenosine in complex}}) + E_{BSSE} \quad (2)$$

$$E_{bind} = E_{\text{Molnupiravir}\cdots\text{Guanosine/Adenosine}} - (E_{\text{Molnupiravir}} + E_{\text{Guanosine/Adenosine}}) + E_{BSSE} \quad (3)$$

where $E_{\text{Molnupiravir}\cdots\text{Guanosine/Adenosine}}$, $E_{\text{Molnupiravir in complex}}$, and $E_{\text{Guanosine/Adenosine in complex}}$ refer to, in consecutive, energies of the complex, molnupiravir drug, and the guanosine/adenosine pertinent to their coordinates in the optimized complexes. $E_{\text{Molnupiravir}}$ and $E_{\text{Guanosine/Adenosine}}$ are energies of the isolated molnupiravir drug and the isolated purine nucleosides, respectively.

Symmetry-adapted perturbation theory (SAPT) calculations were executed to investigate the forces involved in the intermolecular interactions[36] using the PSI4 program package[37] at the SAPT0 level of truncation.[38,39] Within the SAPT analysis, the energies of dispersion ($E_{disp}$), electrostatic ($E_{elst}$), exchange ($E_{exch}$), and induction ($E_{ind}$) were calculated. For the most proficient complexes, total SAPT0 energies were assessed via the following equation (eq 4):[40]

$$E_{SAPT0} = E_{elst} + E_{ind} + E_{disp} + E_{exch} \quad (4)$$

where

$$E_{disp} = E_{disp}^{(20)} + E_{\text{exch-disp}}^{(20)}$$

$$E_{elst} = E_{elst}^{(10)}$$

$$E_{exch} = E_{exch}^{(10)}$$

$$E_{ind} = E_{\text{ind,resp}}^{(20)} + E_{\text{exch-ind,resp}}^{(20)} + \delta_{HF}^{(2)}$$

The calculations of attractive force percent ($E_{\text{attractive}}^{\%}$) were conducted to manifest the contribution of the attractive force ($E_{\text{attractive component}}$), namely, dispersion ($E_{disp}^{\%}$), electrostatic ($E_{elst}^{\%}$), and induction ($E_{ind}^{\%}$), to the total attractive forces ($E_{\text{total attractive forces}}$) via eq 5.

$$E_{\text{attractive}}^{\%} = (E_{\text{attractive component}}/E_{\text{total attractive forces}}) \times 100 \quad (5)$$

The QTAIM analyses accompanied by the NCI index were performed to investigate the interaction nature within the selected complexes. Regarding the QTAIM calculations, the topological features were evaluated by generating bond paths (BPs) and bond critical points (BCPs). The diversity of topological features was also appraised. The NCI diagrams were three-dimensionally plotted using sign($\lambda_2$)$\rho$ with values ranging from −0.035 to 0.020 au (blue to red color coded). The QTAIM and NCI index calculations were carried out using Multiwfn 3.7 software,[41] and their extracted diagrams were visualized using the Visual Molecular Dynamics (VMD) program.[42]

The electronic parameters were obtained with the aid of the FMOs theory. Diagrams of the highest occupied molecular orbital (HOMO) and the lowest unoccupied molecular orbital (LUMO) were visualized for the optimized monomers and complexes. Moreover, the Fermi level ($E_{FL}$) energies and LUMO−HOMO energy gaps ($E_{gap}$) were evaluated based on the $E_{HOMO}$ and $E_{LUMO}$ values via eqs 6 and 7, respectively.

$$E_{FL} = E_{HOMO} + \frac{E_{LUMO} - E_{HOMO}}{2} \quad (6)$$

$$E_{gap} = E_{LUMO} - E_{HOMO} \quad (7)$$

Further, the electronic properties, comprising ionization potentials (IP), chemical potentials ($\mu$), electron affinities (EA), global softness ($S$), global hardness ($\eta$), electrophilicity index ($\omega$), and work functions ($\Phi$), were assessed for the optimized monomers and complexes using eqs 8−14. In the work function estimation, the vacuum-level electrostatic potentials ($V_{eL}(+\infty)$) were proposed to be nearly 0.

$$IP \approx -E_{HOMO} \quad (8)$$

$$EA \approx -E_{LUMO} \quad (9)$$

$$\eta = \frac{E_{LUMO} - E_{HOMO}}{2} \quad (10)$$

$$\mu = \frac{E_{LUMO} + E_{HOMO}}{2} \quad (11)$$

$$s = \frac{1}{\eta} \quad (12)$$

$$\omega = \frac{\mu^2}{2\eta} \quad (13)$$

$$\Phi = V_{eL(+\infty)} - E_{FL} \quad (14)$$

Changes in thermodynamic parameters ($\Delta M$), namely, Gibbs free energy ($\Delta G$), enthalpy ($\Delta H$), and entropy ($\Delta S$), were assessed for the selected complexes using eqs 15 and 16.

$$\Delta M = M_{\text{Molnupiravir}\cdots\text{Guanosine/Adenosine}} - (M_{\text{Molnupiravir}} + M_{\text{Guanosine/Adenosine}}) + E_{BSSE} \quad (15)$$

$$\Delta S = -(\Delta G - \Delta H)/T \quad (16)$$

where $M_{\text{Molnupiravir}\cdots\text{Guanosine/Adenosine}}$, $M_{\text{Molnupiravir}}$, and $M_{\text{Guanosine/Adenosine}}$ represent the $G/H$ values of the optimized complexes, molnupiravir, and guanosine/adenosine, respectively. The $\Delta S$ and $T$ represent the entropy change and temperature, respectively.

The polarizable continuum model (PCM)[43] and universal solvation model density (SMD)[44] were utilized to reveal the water solvation effect on the interactions of molnupiravir with the purine nucleosides. The solvation ($\Delta E_{solv}$) energy was assessed for the optimized complexes as the difference between


https://doi.org/10.1021/acsomega.3c03215
ACS Omega 2023, 8, 27553−27565

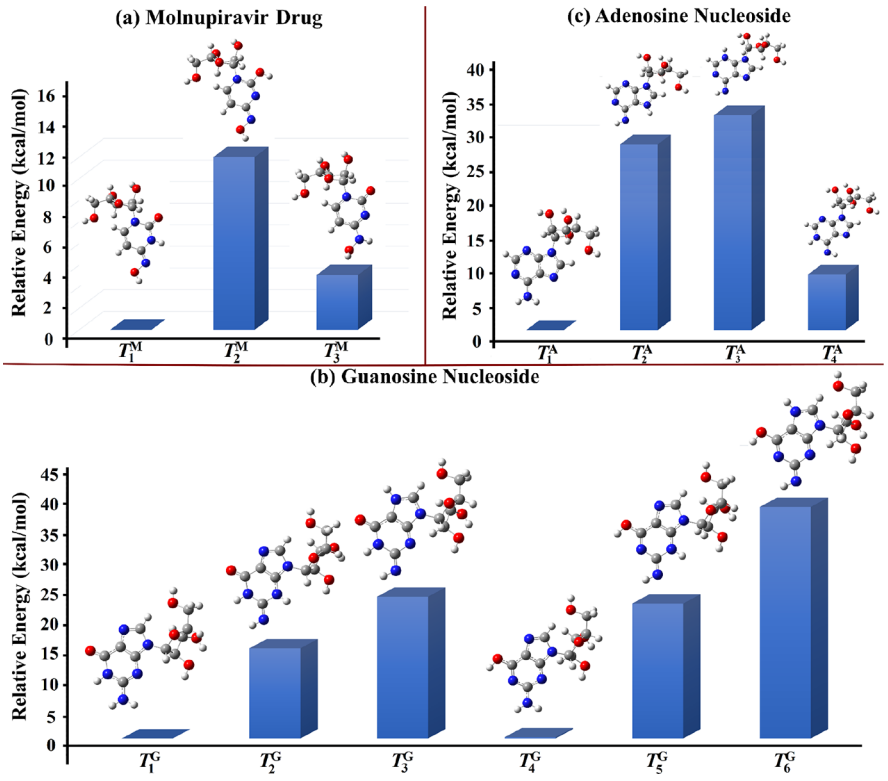


**Figure 2.** Plausible tautomeric structures for the optimized (a) molnupiravir drug, (b) guanosine nucleoside, and (c) adenosine nucleoside.

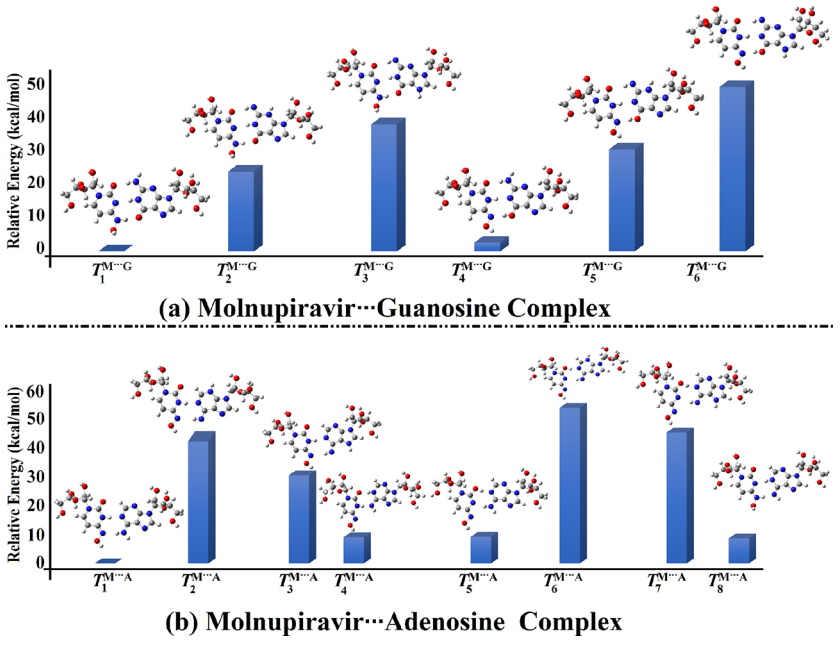


**Figure 3.** Plausible tautomeric structures for the optimized (a) molnupiravir···guanosine (M···G) and (b) molnupiravir···adenosine (M···A) complexes.

the total energies in the water ($E_{solvent}$) and gas ($E_{gas}$) phases according to eq 17.

$$\Delta E_{solv} = E_{solvent} - E_{gas} \quad (17)$$

The Gaussian 09 package[45] was utilized for performing all the employed DFT calculations at the M06-2X/6-311++G(d,p) level of theory.

## RESULTS AND DISCUSSION

**Tautomeric Study.** Toward further inspection for the relative stability of the active form of the molnupiravir drug and its propensity to participate in intermolecular interactions with purine nucleosides, various tautomeric structures were principally idealized. By dint of the presence of a hydroxylamine group, the molnupiravir drug was subjected to amide-iminol tautomerism. Three tautomeric structures, namely,


https://doi.org/10.1021/acsomega.3c03215
ACS Omega 2023, 8, 27553−27565

keto-oxime ($T_1^M$; imino-molnupiravir), hydroxyl-oxime ($T_2^M$), and keto-hydroxylamine ($T_3^M$; amino-molnupiravir), were accordingly obtained.[46] Geometrical optimization supplemented by the relative energy ($E_{relative}$; in kcal/mol) calculations for the plausible tautomeric structures of the molnupiravir drug was performed (see Figure 2).

From Figure 2a, the tautomeric stability of the molnupiravir drug increased according to the succeeding sequence $T_2^M < T_3^M < T_1^M$. Energetically, the imino-molnupiravir ($T_1^M$) was preferred over the amino one ($T_3^M$) by 5.07 kcal/mol. Meanwhile, $T_2^M$ exhibited $E_{relative}$ with respect to $T_1^M$ with a value of 16.00 kcal/mol, which reflected the unfavorability of the hydroxyl-oxime form compared with its analogues. These findings were in coincidence with the beforehand claims.[46]

Regarding the guanosine nucleoside (Figure 2b), the energetic features proclaimed the exaggerated stability of keto-amino ($T_1^G$) and enol-amino ($T_4^G$) forms. Notably, the $E_{relative}$ values showed the unfavorability of keto-($T_2^G$ and $T_3^G$) or enol-($T_5^G$ and $T_6^G$) imino forms compared to the amino ones with values in the range of 15.64−40.16 kcal/mol. Similarly, for adenosine nucleoside, the amino form ($T_1^A$) exhibited paramount stability in comparison to the imino forms ($T_2^A \leftrightarrow T_4^A$) where their $E_{relative}$ recorded about 12.52−35.24 kcal/mol.

Afterward, the plausible tautomeric structures of the drug and nucleosides within the molnupiravir···guanosine and molnupiravir···adenosine complexes were adequately investigated (Figure 3). Geometrical optimization was first executed for the proposed structures followed by the relative energy calculations (Figure 3).

Conspicuously, $E_{relative}$ values accentuated the inclination of the purine bases to exist in the amino form within their interactions (see Figure 3). On the other hand, inimical tautomeric structures were perceived within the imino forms of such bases with the molnupiravir drug. As seen in Figure 3a, the amino and imino forms of the molnupiravir drug showed to be more favorable toward interacting with the keto-amino form ($T_1^{M\cdots G}$) than the enol-amino one ($T_4^{M\cdots G}$) of guanosine by 2.50 kcal/mol. In parallel, among the molnupiravir···adenosine tautomeric structures, $T_1^{M\cdots A}$ was announced as the most proficient one that involves the interactions of the imino-molnupiravir drug with amino-adenosine (see Figure 3b).

Succinctly, the energetic features outlined the most potent complexes to comprise the interactions of amino- and imino-molnupiravir with the keto-amino-guanosine ($T_1^{M\cdots G}$) and amino-adenosine ($T_1^{M\cdots A}$), respectively. Upon the most proficient complexes, sundry DFT computations were conducted to indicate and compare the interactions of the molnupiravir drug with the guanosine and adenosine.

**MEP Analysis.** Graphing the molecular electrostatic potential (MEP) maps offers a visual indication for the distribution of charges over the molecular surfaces of the chemical systems.[47,48] As previously reported, the MEP analysis was executed using an 0.002 au electron density contour toward a good description for the surface of chemical systems.[34,49] MEP maps along with the local most positive and most negative electrostatic potential values ($V_{s,max}$ and $V_{s,min}$) were generated for the preferable tautomeric forms of the molnupiravir drug and the purine nucleosides (Figure 4).

As illustrated in Figure 4, the distribution of the electron densities outlined the electrophilic and nucleophilic natures of the studied molecules by the existence of the blue- and red-colored regions, respectively. The most negative MEP spheres

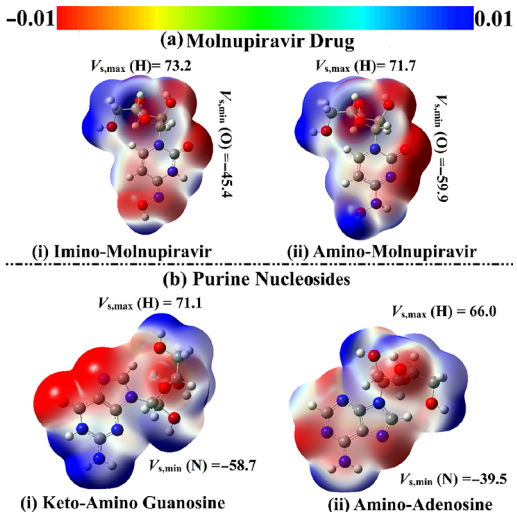


**Figure 4.** MEP maps of the optimized (a) imino and amino forms of the molnupiravir drug along with the (b) purine nucleosides, including keto-amino-guanosine and amino-adenosine. These maps were aligned within the −0.01 and +0.01 au ambit (red to blue colors). The local most positive and most negative electrostatic potential values ($V_{s,max}$ and $V_{s,min}$) are in kcal/mol.

were principally denoted around the surfaces of N and O atoms with elevated sizes for the anterior atom. In contrast, the most positive electrostatic potential was concentrated around the H atoms, announcing the superb versatility toward participating in the hydrogen bonding interactions.

**Energetic Manifestations.** The optimized geometrical structures of the complexes of amino- and imino-molnupiravir with the keto-amino-guanosine and amino-adenosine, respectively, are shown in Figure 5. Table 1 summarizes the values of $E_{int}$, $E_{bind}$, and the intermolecular distances for the investigated complexes.

As depicted in Figure 5, three and two hydrogen bonds (HBs) were remarked within the amino-molnupiravir···keto-amino-guanosine ($T_1^{M\cdots G}$) and imino-molnupiravir···amino-adenosine ($T_1^{M\cdots A}$) complexes, respectively. From Table 1, the distances of the hydrogen bonds were in ranges of 1.75−1.90 and 1.81−2.07 Å within the former and latter complexes, respectively.

Passing to the energetic perspective, higher negative values of the $E_{int}/E_{bind}$ were divulged for the amino-molnupiravir···keto-amino-guanosine ($T_1^{M\cdots G}$) complex than the imino-molnupiravir···amino-adenosine ($T_1^{M\cdots A}$) analogue. Numerically, $E_{int}/E_{bind}$ values were −31.16/−21.81 and −13.93/−12.83 kcal/mol for the former and latter complexes, respectively (Table 1). These observations ensured the higher proficiency of the molnupiravir drug to bind with guanosine compared with the adenosine one. This finding reflected the favorability of the molnupiravir incorporation instead of the cytidine over the uridine in the SARS-CoV-2's RNA replication, which was in line with the literature.[27] Generally, the DFT energetic computations highlighted the opulent efficiency of the molnupiravir drug to interfere with the viral replication, affirming its eminent role as a competitive substrate for the SARS-CoV-2 RdRp.

**SAPT Calculations.** Symmetry-adapted perturbation theory (SAPT) calculations were accomplished for the optimized complexes of amino- and imino-molnupiravir with keto-amino-guanosine and amino-adenosine, respectively,


https://doi.org/10.1021/acsomega.3c03215
ACS Omega 2023, 8, 27553−27565

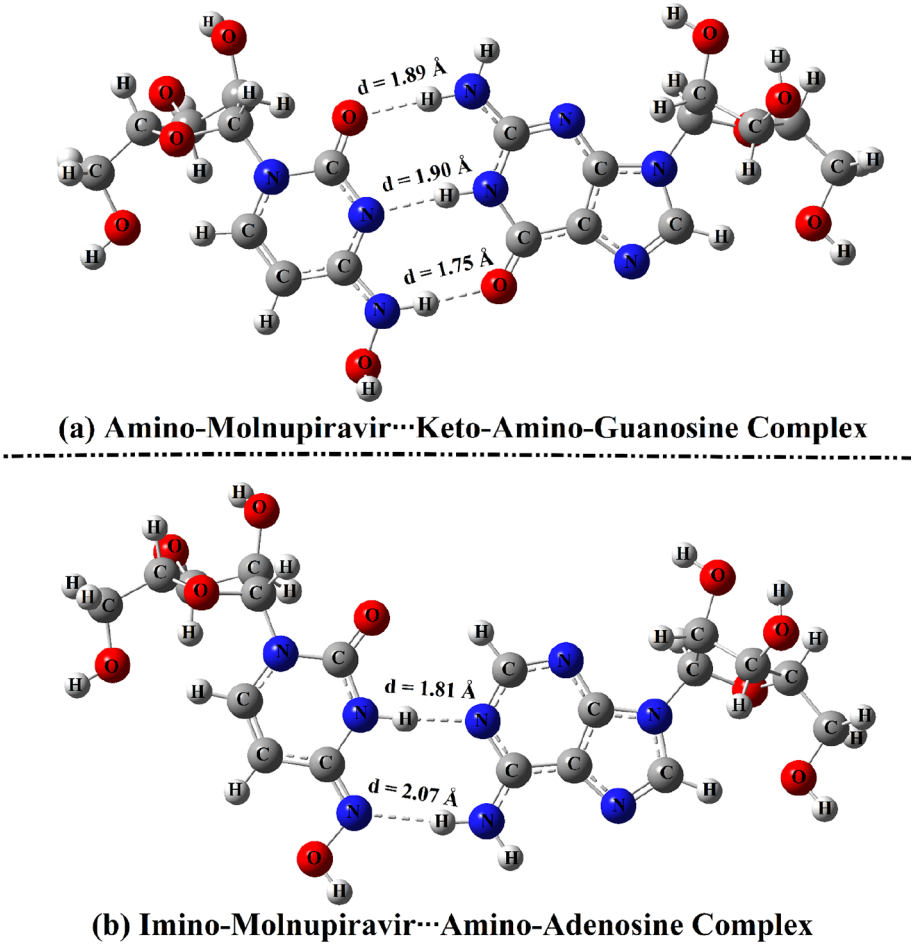


**Figure 5.** Optimized geometrical structures of the (a) amino-molnupiravir···keto-amino-guanosine ($T_1^{M\cdots G}$) and (b) imino-molnupiravir···amino-adenosine ($T_1^{M\cdots A}$) complexes.

**Table 1. Interaction ($E_{int}$) and Binding ($E_{bind}$) Energies (in kcal/mol) of (a) Amino-Molnupiravir···Keto-Amino-Guanosine ($T_1^{M\cdots G}$) and (b) Imino-Molnupiravir···Amino-Adenosine ($T_1^{M\cdots A}$) Complexes**[a]

| (a) Amino-molnupiravir···keto-amino-guanosine ($T_1^{m\cdots g}$) complex | | | |
|---|---|---|---|
| HB type | distance (Å) | $E_{int}$ (kcal/mol) | $E_{bind}$ (kcal/mol) |
| O···H | 1.89 | −31.16 | −21.81 |
| N···H | 1.90 | | |
| H···O | 1.75 | | |
| (b) Imino-molnupiravir···amino-adenosine ($T_1^{m\cdots a}$) complex | | | |
| HB type | distance (Å) | $E_{int}$ (kcal/mol) | $E_{bind}$ (kcal/mol) |
| H···N | 1.81 | −13.93 | −12.83 |
| N···H | 2.07 | | |

[a]Intermolecular distances of the obtained hydrogen bonds (HBs) are given in Å.

using the PSI4 code.[34] Within SAPT analysis, the total interaction energy was dissected into its main energetic components, dubbed dispersion ($E_{disp}$), electrostatic ($E_{elst}$), exchange ($E_{exch}$), and induction ($E_{ind}$) forces at the SAPT0 level of truncation. The obtained attractive and repulsive components are correlated in bar charts (Figure 6). In addition, the calculations of attractive force percent ($E^{\%}_{attractive}$) were performed to illustrate the contributions of the obtained attractive components, namely, $E^{\%}_{disp}$, $E^{\%}_{elst}$, and $E^{\%}_{ind}$, to the total attractive forces and are graphed in Figure 6.

The bar charts shown in Figure 6 announced negative energetic values for the dispersion ($E_{disp}$), electrostatic ($E_{elst}$), and induction ($E_{ind}$) forces, shedding light on their role in stabilizing the investigated molnupiravir···purine nucleoside complexes. Further, bar charts outlined the prevalence of the interactions of the molnupiravir drug with guanosine and adenosine by the $E_{elst}$. Conspicuously, a more negative value for such predominant $E_{elst}$ was registered for the amino-molnupiravir···keto-amino-guanosine ($T_1^{M\cdots G}$) over the imino-molnupiravir···amino-adenosine ($T_1^{M\cdots A}$) analogue that coincided with $E_{int}/E_{bind}$ results (Table 1). Illustratively, for the former and latter complexes, $E_{elst}$ were −45.65 and −26.99 kcal/mol, along with $E_{int}/E_{bind}$ of −31.16/−21.81 and −13.93/−12.83 kcal/mol, respectively. In addition, elevated negative $E_{disp}$ and $E_{ind}$ were disclosed, enlightening their reputable contributions to the stabilization of the molnupiravir···purine nucleoside complexes. On the contrary, unfavorable repulsive contributions to the total SAPT0 energy were recorded for the $E_{exch}$ component of the investigated complexes. For example, values of $E_{disp}$, $E_{ind}$, and $E_{exch}$ of the amino-molnupiravir···keto-amino-guanosine ($T_1^{M\cdots G}$) complex were −12.35, −19.60, and 40.23 kcal/mol, respectively.

Moreover, the pie chart shown in Figure 6 demonstrates the supreme contribution of the electrostatic component to the total attractive forces. Numerically, the $E^{\%}_{elst}$ recorded about 59 and 57% of the total attractive forces of the amino-molnupiravir···keto-amino-guanosine ($T_1^{M\cdots G}$) and imino-


https://doi.org/10.1021/acsomega.3c03215
ACS Omega 2023, 8, 27553−27565

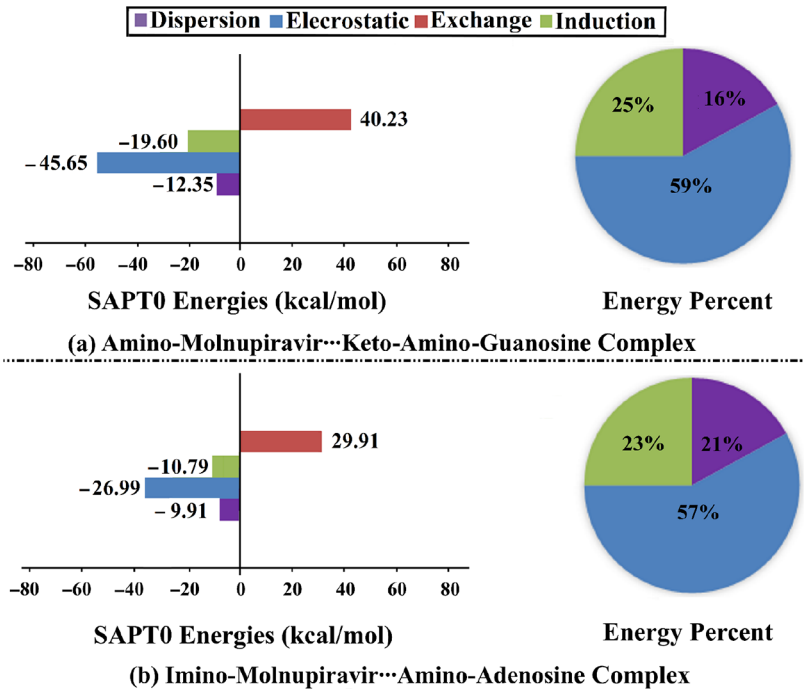


**Figure 6.** Bar charts of the principal energetic components of total SAPT0 energy, namely, dispersion ($E_{disp}$), electrostatic ($E_{elst}$), exchange ($E_{exch}$), and induction ($E_{ind}$) forces for the (a) amino-molnupiravir···keto-amino-guanosine ($T_1^{M\cdots G}$) and (b) imino-molnupiravir···amino-adenosine ($T_1^{M\cdots A}$) complexes. The pie chart of the attractive force percent with respect to the total attractive forces.

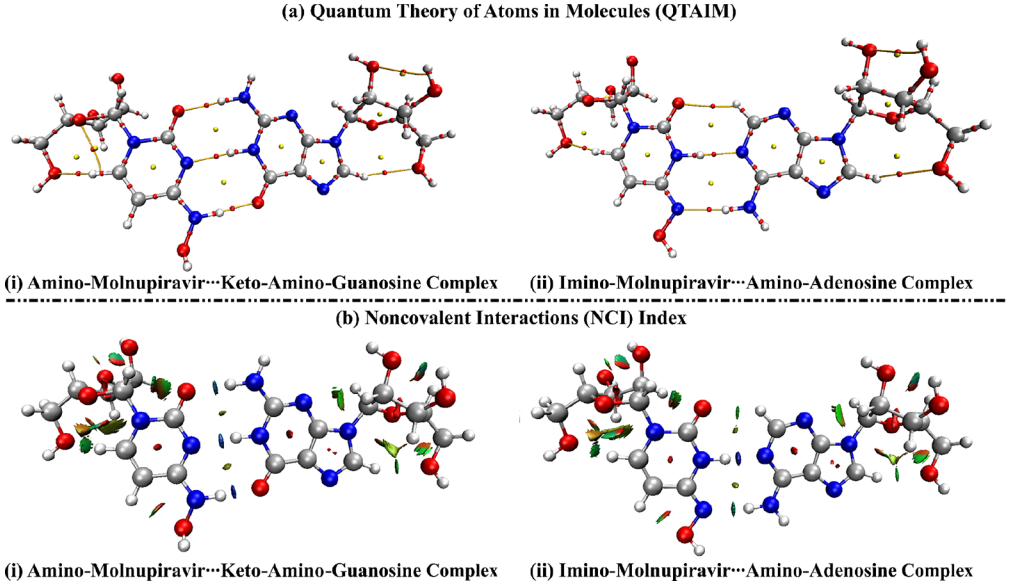


**Figure 7.** (a) QTAIM and (b) 3D NCI schemes of the amino-molnupiravir···keto-amino-guanosine ($T_1^{M\cdots G}$) and the imino-molnupiravir···amino-adenosine ($T_1^{M\cdots A}$) optimized complexes. Red dots indicate the location of BCPs and BPs. Isosurfaces of NCI plots are shown with a reduced density gradient value of 0.50 au. The color range is set with respect to the sign($\lambda_2$)$\rho$ from blue (−0.035) to red (0.020) au.

molnupiravir···amino-adenosine ($T_1^{M\cdots A}$) complexes, respectively. For both complexes, the attractive force percent ($E^{\%}$) manifestations proclaimed the contributions of the considered attractive forces according to the successive order $E^{\%}_{disp} < E^{\%}_{ind} < E^{\%}_{elst}$. For instance, $E^{\%}_{disp}/E^{\%}_{ind}/E^{\%}_{elst}$ were about 16/25/59 and 21/23/57% of the total attractive forces within amino-molnupiravir···keto-amino-guanosine ($T_1^{M\cdots G}$) and the imino-molnupiravir···amino-adenosine ($T_1^{M\cdots A}$) complexes, respectively. Overall, these findings principally outlined the electrostatic nature of the scouted interactions of the molnupiravir drug with the purine nucleosides.

**QTAIM and NCI Analyses.** Quantum theory of atoms in molecules (QTAIM) and noncovalent interaction (NCI) index analyses were earlier authenticated to be a trusty appliance to inspect the intra- and inter-molecular interactions.[50−52] In accordance, the interactions of the molnupiravir drug with the purine nucleosides were elucidated from the QTAIM and NCI viewpoints in reliance on the electron density features. Figure 7 involves QTAIM and NCI diagrams for the optimized complexes of amino- and imino-molnupiravir with keto-amino-guanosine and amino-adenosine, respectively. Table 2 enrolls the QTAIM topological parameters, including total


https://doi.org/10.1021/acsomega.3c03215
ACS Omega 2023, 8, 27553−27565

Table 2. Topological Parameters of the (a) Amino-Molnupiravir···Keto-Amino-Guanosine ($T_1^{M\cdots G}$) and the (b) Imino-Molnupiravir···Amino-Adenosine ($T_1^{M\cdots A}$) Optimized Complexes[a]

| (a) Amino-molnupiravir···keto-amino-guanosine ($T_1^{m\cdots g}$) complex | | | | | | |
|---|---|---|---|---|---|---|
| HB type | $\rho_b$ | $H_b$ | $\nabla^2\rho_b$ | $G_b$ | $V_b$ | $-G_b/V_b$ |
| O···H | 0.0270 | 0.0022 | 0.1058 | 0.0242 | −0.0220 | 1.1016 |
| N···H | 0.0327 | −0.0006 | 0.0966 | 0.0248 | −0.0255 | 0.9745 |
| H···O | 0.0383 | −0.0011 | 0.1321 | 0.0341 | −0.0352 | 0.9693 |
| (b) Imino-molnupiravir···amino-adenosine ($T_1^{m\cdots a}$) complex | | | | | | |
| HB type | $\rho_b$ | $H_b$ | $\nabla^2\rho_b$ | $G_b$ | $V_b$ | $-G_b/V_b$ |
| H···N | 0.0416 | −0.0049 | 0.1024 | 0.0305 | −0.0355 | 0.8609 |
| N···H | 0.0220 | 0.0021 | 0.0746 | 0.0165 | −0.0144 | 1.1455 |

[a]All parameters are in au.

energy density ($H_b$), electron density ($\rho_b$), Laplacian ($\nabla^2\rho_b$), local potential electron energy density ($V_b$), kinetic electron density ($G_b$), and the negative ratio of kinetic and potential electron energy density ($-G_b/V_b$).

From QTAIM schemes in Figure 7a, the intermolecular space between the molnupiravir drug and the purine nucleosides was characterized by the presence of a set of BCPs and BPs. This observation demonstrated the occurrence of favorable interactions within the investigated complexes. Further, QTAIM schemes illustrated the favorability of the molnupiravir drug to bind with the guanosine over the adenosine analogue, through the existence of three and two main BCPs and BPs (i.e., hydrogen bonds), respectively. Astonishingly, the QTAIM scheme disclosed the presence of the C−H···O hydrogen bond for the imino-molnupiravir···amino-adenosine ($T_1^{M\cdots A}$) complex; in turn, it participated in stabilizing such complex, albeit within weaker contributions. This opulent contributing role for the structural stability relevant to this unconventional hydrogen bond was previously outlined in literature.[53]

Quantitively, the successive findings were perceived for almost all the intermolecular interactions within the investigated complexes: negative $H_b$ values, positive $\nabla^2\rho_b$ values, and $-G_b/V_b$ values less than the unity, outlining the partially covalent nature of the interactions involved between the molnupiravir drug and purine nucleosides (Table 2). For example, values of $H_b$, $\nabla^2\rho_b$, and $-G_b/V_b$ were −0.0011, 0.1321, and 0.9693 au, respectively, for the N···H bond within the amino-molnupiravir···keto-amino-guanosine ($T_1^{M\cdots G}$) complex.

According to Figure 7b, three and two blue-colored surfaces (i.e., maximal attractive forces) within the amino-molnupiravir···keto-amino-guanosine ($T_1^{M\cdots G}$) and imino-molnupiravir···amino-adenosine ($T_1^{M\cdots A}$) optimized complexes were disclosed, respectively. Accordingly, the NCI schemes also reflected the versatility of the molnupiravir drug toward interacting with purine nucleosides. Evidently, in synchrony with the QTAIM claims, NCI schemes assured the weak contributions of the unconventional C−H···O hydrogen bond into stabilizing the imino-molnupiravir···amino-adenosine ($T_1^{M\cdots A}$) complex via the presence of a green-colored surface.

**Electronic Parameters.** In the current study, FMOs theory was devoted to elucidating the electronic structure changes in the interaction of molnupiravir with the purine nucleosides. Quantitatively, energies of the highest occupied molecular orbital ($E_{HOMO}$) and the lowest unoccupied molecular orbital ($E_{LUMO}$) along with the Fermi level ($E_{FL}$) and energy gap ($E_{gap}$) were calculated for the amino-molnupiravir···keto-amino-guanosine ($T_1^{M\cdots G}$) and imino-molnupiravir···amino-adenosine ($T_1^{M\cdots A}$) complexes and their isolated systems (Table 3). Figure S1 and Figure 8 display the HOMO/LUMO electron densities for the isolated systems and complexes, respectively. Table 3 involves the $E_{HOMO}$, $E_{LUMO}$, $E_{FL}$, and $E_{gap}$ values.

Table 3. (a, b) Electronic Parameters for the Imino and Amino Forms of the Molnupiravir Drug along with the Keto-Amino-Guanosine and Amino-Adenosine before and after Interaction within the Amino-Molnupiravir···Keto-Amino-Guanosine ($T_1^{M\cdots G}$) and Imino-Molnupiravir···Amino-Adenosine ($T_1^{M\cdots A}$) Complexes (in eV)

| (a) Systems | | | |
|---|---|---|---|
| $E_{HOMO}$ (eV) | $E_{LUMO}$ (eV) | $E_{FL}$ (eV) | $E_{gap}$ (eV) |
| (i) Imino-molnupiravir | | | |
| −7.177 | −0.570 | −3.873 | 6.608 |
| (ii) Amino-molnupiravir | | | |
| −7.801 | −0.570 | −4.186 | 7.231 |
| (iii) Keto-amino-guanosine | | | |
| −7.260 | −0.670 | −3.965 | 6.589 |
| (iv) Amino-adenosine | | | |
| −7.480 | −0.294 | −3.887 | 7.186 |
| (b) Complex | | | |
| $E_{HOMO}$ (eV) | $E_{LUMO}$ (eV) | $E_{FL}$ (eV) | $E_{gap}$ (eV) |
| (i) Amino-molnupiravir···keto-amino-Guanosine ($T_1^{M\cdots G}$) complex | | | |
| −6.678 | −0.665 | −3.672 | 6.013 |
| (ii) Imino-molnupiravir···amino-adenosine ($T_1^{M\cdots A}$) complex | | | |
| −7.075 | −0.509 | −3.792 | 6.566 |

As shown in Figure S1, the distributions of HOMO were noticed over the ring of the molnupiravir drug and purine nucleosides. In comparison, the LUMO levels surrounded the other part of the studied isolated systems. Turning to the amino-molnupiravir···keto-amino-guanosine ($T_1^{M\cdots G}$) and imino-molnupiravir···amino-adenosine ($T_1^{M\cdots A}$), the distributions of HOMO and LUMO were dramatically changed, compared to the isolated systems (see Figure 8). This finding validated the prominent role of charge transfer beyond the occurrence of the investigated interactions.

From Table 3, the $E_{HOMO}$, $E_{LUMO}$, $E_{FL}$, and $E_{gap}$ values were notably changed before and after interactions of the amino- and imino-molnupiravir drug with the keto-amino-guanosine and amino-adenosine, respectively. Numerically, the $E_{HOMO}/E_{LUMO}/E_{FL}/E_{gap}$ values were −7.260/−0.670/−3.965/6.589 and −6.678/−0.665/−3.672/6.013 eV for the isolated keto-amino-guanosine and the amino-molnupiravir···keto-amino-guanosine ($T_1^{M\cdots G}$) complex, respectively.

**Global Indices of Reactivity.** Global reactivity indices, comprising ionization potentials (IP), electron affinities (EA), chemical potentials ($\mu$), global hardness ($\eta$), global softness ($S$), electrophilicity index ($\omega$), and work functions ($\Phi$), were assessed to uncover the change in the electronic properties resulting from the molnupiravir interactions with the purine nucleosides (Table 4).

Upon the complexation of the molnupiravir drug with purine nucleosides, remarkable changes in the studied reactivity parameters were perceived (Table 4). Obviously,


https://doi.org/10.1021/acsomega.3c03215
ACS Omega 2023, 8, 27553−27565

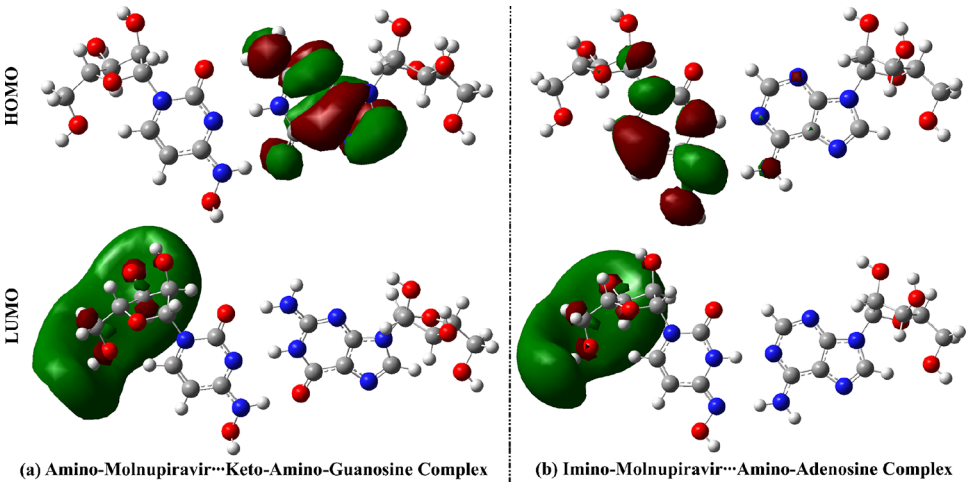


**Figure 8.** HOMO and LUMO plots of the (a) amino-molnupiravir···keto-amino-guanosine ($T_1^{M\cdots G}$) and (b) imino-molnupiravir···amino-adenosine ($T_1^{M\cdots A}$) optimized complexes.

**Table 4. (a, b) Global Indices of Reactivity of the Optimized Imino and Amino Forms of the Molnupiravir Drug along with the Keto-Amino-Guanosine and Amino-Adenosine before and after Interaction (in eV)**

| (a) Systems | | | | | | |
|---|---|---|---|---|---|---|
| IP (eV) | EA (eV) | $\mu$ (eV) | $\eta$ (eV) | $S$ ($eV^{-1}$) | $\omega$ (eV) | $\Phi$ (eV) |
| (i) Imino-molnupiravir | | | | | | |
| 7.177 | 0.570 | −3.873 | 3.304 | 0.303 | 2.271 | 3.873 |
| (ii) Amino-molnupiravir | | | | | | |
| 7.801 | 0.570 | −4.186 | 3.616 | 0.277 | 2.423 | 4.186 |
| (iii) Keto-amino-guanosine | | | | | | |
| 7.260 | 0.670 | −3.965 | 3.295 | 0.304 | 2.386 | 3.965 |
| (iv) Amino-adenosine | | | | | | |
| 7.480 | 0.294 | −3.887 | 3.593 | 0.278 | 2.103 | 3.887 |
| (b) Complex | | | | | | |
| IP (eV) | EA (eV) | $\mu$ (eV) | $\eta$ (eV) | $S$ ($eV^{-1}$) | $\omega$ (eV) | $\Phi$ (eV) |
| (i) Amino-molnupiravir···keto-amino-guanosine ($T_1^{M\cdots G}$) complex | | | | | | |
| 6.678 | 0.665 | −3.672 | 3.007 | 0.333 | 2.242 | 3.672 |
| (ii) Imino-molnupiravir···amino-adenosine ($T_1^{M\cdots A}$) complex | | | | | | |
| 7.075 | 0.509 | −3.792 | 3.283 | 0.305 | 2.189 | 3.792 |

the IP, $\mu$, $\eta$, and $\Phi$ values of the isolated systems were found to decrease in the complexed forms, and vice versa was true for the $S$ values. Meanwhile, an irregular pattern was denoted for the EA and $\omega$ values. Illustratively, the IP value was 7.260 eV for the keto-amino-guanosine and diminished to 6.678 eV after its interactions with the amino-molnupiravir. The anomalous behavior of EA and $\omega$ values might be explained as an upshot to its dependence on the $E_{LUMO}$ value.

**Thermodynamic Parameters.** Interactions of the molnupiravir drug with the purine nucleosides were scrutinized from a thermodynamic viewpoint. Figure 9 displays the changes in thermodynamic quantities of the amino-molnupiravir···keto-amino-guanosine ($T_1^{M\cdots G}$) and imino-molnupiravir···amino-adenosine ($T_1^{M\cdots A}$) optimized complexes.

As evident in Figure 9, negative $\Delta G$ and $\Delta H$ values were recorded for the amino-molnupiravir···keto-amino-guanosine ($T_1^{M\cdots G}$) and imino-molnupiravir···amino-adenosine ($T_1^{M\cdots A}$) optimized complexes. This observation accordingly demonstrated the spontaneous and exothermic nature of the scouted interactions. In addition, both molnupiravir···purine

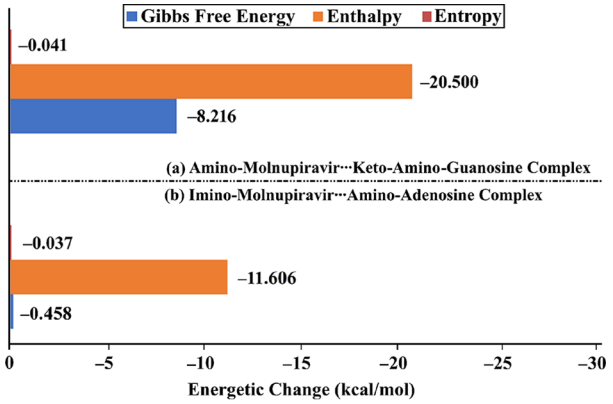


**Figure 9.** Energetic change (in kcal/mol) of the thermodynamic parameters for the (a) amino-molnupiravir···keto-amino-guanosine ($T_1^{M\cdots G}$) and (b) imino-molnupiravir···amino-adenosine ($T_1^{M\cdots A}$) optimized complexes.

nucleoside complexes exhibited small negative $\Delta S$ values that suggested debilitating the randomness of the studied interactions. In synchrony with the energetic observations (Table 1), more favorable $\Delta G$, $\Delta H$, and $\Delta S$ considerations with higher negative values were ascribed to the amino-molnupiravir···keto-amino-guanosine ($T_1^{M\cdots G}$) complex against the imino-molnupiravir···amino-adenosine ($T_1^{M\cdots A}$) counterpart. This observation illustrated more proficiency of the molnupiravir drug to interact with the keto-amino-guanosine than the amino-adenosine. Illustratively, the $\Delta G/\Delta H/\Delta S$ values of the amino-molnupiravir···keto-amino-guanosine ($T_1^{M\cdots G}$) and imino-molnupiravir···amino-adenosine ($T_1^{M\cdots A}$) were −8.216/−20.500/−0.041 and −0.458/−11.606/−0.037 kcal/mol.

**Solvent Effect.** Using the polarizable continuum model (PCM)[43] and universal solvation model density (SMD),[44] the solvent effect on the interactions of the molnupiravir with purine nucleosides was assessed and comparatively investigated. Geometrical optimization computations were first carried out for the amino-molnupiravir···keto-amino-guanosine ($T_1^{M\cdots G}$) and imino-molnupiravir···amino-adenosine ($T_1^{M\cdots A}$) complexes in a water medium. For the obtained structures, the interaction ($E_{int}$) and binding ($E_{bind}$) energies were calculated (Table 5).


https://doi.org/10.1021/acsomega.3c03215
ACS Omega 2023, 8, 27553−27565

Table 5. Interaction ($E_{int}$) and Binding ($E_{bind}$) for the (a) Amino-Molnupiravir···Keto-Amino-Guanosine ($T_1^{M\cdots G}$) and (b) Imino-Molnupiravir···Amino-Adenosine ($T_1^{M\cdots A}$) Optimized Complexes in the Water Medium[a]

| | (a) Amino-molnupiravir···keto-amino-guanosine ($T_1^{m\cdots g}$) complex | | | | | | | |
|---|---|---|---|---|---|---|---|---|
| | PCM | | | | SMD | | | |
| HB type | distance | $E_{int}$ | $E_{bind}$ | $\Delta E_{solv}$[a] | distance | $E_{int}$ | $E_{bind}$ | $\Delta E_{solv}$[a] |
| O···H | 1.87 | −16.06 | −13.63 | −28.98 | 1.90 | −9.20 | −8.84 | −53.38 |
| N···H | 1.90 | | | | 1.95 | | | |
| H···O | 1.84 | | | | 1.88 | | | |
| | (b) Imino-molnupiravir···amino-adenosine ($T_1^{M\cdots A}$) complex | | | | | | | |
| | PCM | | | | SMD | | | |
| HB type | distance | $E_{int}$ | $E_{bind}$ | $\Delta E_{solv}$[a] | distance | $E_{int}$ | $E_{bind}$ | $\Delta E_{solv}$[a] |
| H···N | 1.84 | −9.82 | −9.12 | −24.67 | 1.88 | −5.92 | −5.40 | −48.11 |
| N···H | 2.04 | | | | 2.07 | | | |

[a]Solvation energy ($\Delta E_{solv}$) was calculated according to eq 17 (i.e., $\Delta E_{solv} = E_{solvent} - E_{gas}$). Intermolecular distances of the obtained hydrogen bonds (HBs) are given in Å with the incorporation of the polarizable continuum model (PCM) and universal solvation model density (SMD).

As given in Table 5, negative energetic values were denoted for the optimized complexes in the presence of the water solvent. In line with the gas phase, more negative $E_{int}/E_{bind}$ values were perceived for the amino-molnupiravir···keto-amino-guanosine ($T_1^{M\cdots G}$) than the imino-molnupiravir···amino-adenosine ($T_1^{M\cdots A}$) optimized complexes in the water medium. Illustratively, with the incorporation of PCM, the $E_{int}/E_{bind}$ values were −16.06/−13.63 and −9.82/−9.12 kcal/mol for amino-molnupiravir···keto-amino-guanosine ($T_1^{M\cdots G}$) and imino-molnupiravir···amino-adenosine ($T_1^{M\cdots A}$) optimized complexes in the water medium, respectively.

Apparently, negative $\Delta E_{solv}$ values were observed, indicating the opulent role of the water solvent in enhancing the studied interactions compared to the gas phase. Conspicuously, the utilization of SMD showed higher negative solvation energy in comparison to the PCM counterpart, with more observable negative values in the case of the amino-molnupiravir···keto-amino-guanosine ($T_1^{M\cdots G}$) complex. Quantitatively, with the employment of the PCM/SMD, $\Delta E_{solv}$ were −28.98/−53.38 and −24.67/−48.11 kcal/mol for the amino-molnupiravir···keto-amino-guanosine ($T_1^{M\cdots G}$) and imino-molnupiravir···amino-adenosine ($T_1^{M\cdots A}$) complexes, respectively.

## CONCLUSIONS

Herein, the preferability of the molnupiravir in its active form toward interacting with the guanosine and adenosine nucleosides was investigated using a broad set of DFT calculations. Upon investigating the plausible tautomeric structures of the scouted drug and purine nucleosides, the energetic stability could be concluded as follows: (i) for the molnupiravir drug, the imino ($T_1^M$) form demonstrated more noticeable stability compared with the amino ($T_3^M$) one by 5.07 kcal/mol, (ii) for guanosine, the energetic features proclaimed the exaggerated stability of keto-amino and enol-amino forms, and (iii) for adenosine, the amino form showed higher stability than the imino forms where their $E_{relative}$ recorded in the range of 12.52−35.24 kcal/mol. Upon the obtained findings from the tautomerization effect on the base-pairing efficiency, the most potent complexes were ascribed to the interactions of amino- and imino-molnupiravir with the keto-amino-guanosine and amino-adenosine, respectively. Notable changes in the electronic properties and global indices of reactivity were observed for the most stable molnupiravir···purine nucleoside complexes in comparison to their isolated systems. Also, the partially covalent nature of molnupiravir···purine interactions was announced in terms of QTAIM and NCI observations. Based on thermodynamic parameters, the spontaneous, exothermic, and nonrandom states of the molnupiravir···purine interactions were highlighted. Apparently, the eminent bias of the molnupiravir drug to bind more favorably with the guanosine over the adenosine one was assured, reflecting the more efficient incorporation of molnupiravir instead of cytidine than uridine in the SARS-CoV-2's RNA replication. Favorability of guanosine-based complexes over adenosine analogues was also noticed in the water medium. The obtained manifestations would be a plentiful reference to the incoming research concerned with the interactions of the molnupiravir drug with purine nucleosides.

## ASSOCIATED CONTENT

### Supporting Information

The Supporting Information is available free of charge at https://pubs.acs.org/doi/10.1021/acsomega.3c03215.

HOMO and LUMO plots for the molnupiravir drug and purine nucleosides (PDF)

## AUTHOR INFORMATION


### Corresponding Authors

**Mahmoud A. A. Ibrahim** − *Computational Chemistry Laboratory, Chemistry Department, Faculty of Science, Minia University, Minia 61519, Egypt; School of Health Sciences, University of KwaZulu-Natal, Durban 4000, South Africa;* orcid.org/0000-0003-4819-2040; Email: m.ibrahim@compchem.net

**Tamer Shoeib** − *Department of Chemistry, The American University in Cairo, New Cairo 11835, Egypt;* orcid.org/0000-0003-3512-1593; Email: t.shoeib@aucegypt.edu

### Authors

**Mohammed N. I. Shehata** − *Computational Chemistry Laboratory, Chemistry Department, Faculty of Science, Minia University, Minia 61519, Egypt;* orcid.org/0000-0002-3334-6070

**Nayra A. M. Moussa** − *Computational Chemistry Laboratory, Chemistry Department, Faculty of Science, Minia University, Minia 61519, Egypt;* orcid.org/0000-0003-3712-7710

**Randa R. A. Hemia** − *Computational Chemistry Laboratory, Chemistry Department, Faculty of Science, Minia University, Minia 61519, Egypt*




https://doi.org/10.1021/acsomega.3c03215
ACS Omega 2023, 8, 27553−27565

**Heba S. M. Abd Elhafez** − *Computational Chemistry Laboratory, Chemistry Department, Faculty of Science, Minia University, Minia 61519, Egypt*
**Mohamed K. Abd El-Rahman** − *Department of Chemistry and Chemical Biology, Harvard University, Cambridge, Massachusetts 02138, United States*
**Shaban R. M. Sayed** − *Department of Botany and Microbiology, College of Science, King Saud University, Riyadh 11451, Saudi Arabia*
**Peter A. Sidhom** − *Department of Pharmaceutical Chemistry, Faculty of Pharmacy, Tanta University, Tanta 31527, Egypt;* orcid.org/0000-0003-2579-6351
**Eslam Dabbish** − *Department of Chemistry, The American University in Cairo, New Cairo 11835, Egypt;* orcid.org/0000-0002-3601-0193

Complete contact information is available at: https://pubs.acs.org/10.1021/acsomega.3c03215

### Author Contributions

M.A.A.I.: Conceptualization, methodology, software, resources, project administration, supervision, and writing—review and editing. M.N.I.S.: Data curation, formal analysis, investigation, visualization, and writing—original draft. N.A.M.M.: Methodology, investigation, project administration, and writing—review and editing. R.R.A.H.: Visualization. H.S.M.A.E.: Formal analysis. M.K.A.E.-R.: Writing—review and editing. S.R.M.S.: Resources and writing—review and editing. P.A.S.: Visualization and writing—review and editing. E.D.: Investigation and writing—review and editing. T.S.: Conceptualization, resources, and writing—review and editing.

### Notes

The authors declare no competing financial interest.

## ■ ACKNOWLEDGMENTS

The authors extend their appreciation to the Researchers Supporting Project number (RSPD2023R743), King Saud University, Riyadh, Saudi Arabia, for funding this work. The computational work was completed with resources provided by the Science and Technology Development Fund (STDF-Egypt, grants nos. 5480 and 7972), Bibliotheca Alexandrina (http://hpc.bibalex.org), and the American University in Cairo. M.A.A.I. extends his appreciation to the Academy of Scientific Research and Technology (ASRT, Egypt) for funding the Graduation Projects conducted at CompChem Lab, Egypt.

## ■ REFERENCES

(1) Wu, F.; Zhao, S.; Yu, B.; Chen, Y. M.; Wang, W.; Song, Z. G.; Hu, Y.; Tao, Z. W.; Tian, J. H.; Pei, Y. Y.; Yuan, M. L.; Zhang, Y. L.; Dai, F. H.; Liu, Y.; Wang, Q. M.; Zheng, J. J.; Xu, L.; Holmes, E. C.; Zhang, Y. Z. A new coronavirus associated with human respiratory disease in China. *Nature* **2020**, *579*, 265−269.
(2) Almeida-Leite, C. M.; Stuginski-Barbosa, J.; Conti, P. C. R. How psychosocial and economic impacts of COVID-19 pandemic can interfere on bruxism and temporomandibular disorders? *J. Appl. Oral Sci.* **2020**, *28*, No. e20200263.
(3) Lanham-New, S. A.; Webb, A. R.; Cashman, K. D.; Buttriss, J. L.; Fallowfield, J. L.; Masud, T.; Hewison, M.; Mathers, J. C.; Kiely, M.; Welch, A. A.; Ward, K. A.; Magee, P.; Darling, A. L.; Hill, T. R.; Greig, C.; Smith, C. P.; Murphy, R.; Leyland, S.; Bouillon, R.; Ray, S.; Kohlmeier, M. Vitamin D and SARS-CoV-2 virus/COVID-19 disease. *BMJ Nutr. Prev. Health* **2020**, *3*, 106−110.
(4) Zheng, M.; Gao, Y.; Wang, G.; Song, G.; Liu, S.; Sun, D.; Xu, Y.; Tian, Z. Functional exhaustion of antiviral lymphocytes in COVID-19 patients. *Cell. Mol. Immunol.* **2020**, *17*, 533−535.
(5) Pal, M.; Berhanu, G.; Desalegn, C.; Kandi, V. Severe Acute Respiratory Syndrome Coronavirus-2 (SARS-CoV-2): An Update. *Cureus* **2020**, *12*, No. e7423.
(6) Yan, S.; Sun, H.; Bu, X.; Wan, G. New Strategy for COVID-19: An Evolutionary Role for RGD Motif in SARS-CoV-2 and Potential Inhibitors for Virus Infection. *Front. Pharmacol.* **2020**, *11*, 912.
(7) Lan, J.; Ge, J.; Yu, J.; Shan, S.; Zhou, H.; Fan, S.; Zhang, Q.; Shi, X.; Wang, Q.; Zhang, L.; Wang, X. Structure of the SARS-CoV-2 spike receptor-binding domain bound to the ACE2 receptor. *Nature* **2020**, *581*, 215−220.
(8) Jackson, C. B.; Farzan, M.; Chen, B.; Choe, H. Mechanisms of SARS-CoV-2 entry into cells. *Nat. Rev. Mol. Cell Biol.* **2022**, *23*, 3−20.
(9) Luan, B.; Huynh, T.; Cheng, X.; Lan, G.; Wang, H. R. Targeting Proteases for Treating COVID-19. *J. Proteome Res.* **2020**, *19*, 4316−4326.
(10) Mahmoudvand, S.; Shokri, S. Interactions between SARS coronavirus 2 papain-like protease and immune system: A potential drug target for the treatment of COVID-19. *Scand. J. Immunol.* **2021**, *94*, No. e13044.
(11) Singh, R.; Bhardwaj, V. K.; Sharma, J.; Kumar, D.; Purohit, R. Identification of potential plant bioactive as SARS-CoV-2 Spike protein and human ACE2 fusion inhibitors. *Comput. Biol. Med.* **2021**, *136*, No. 104631.
(12) Pandey, P.; Rane, J. S.; Chatterjee, A.; Kumar, A.; Khan, R.; Prakash, A.; Ray, S. Targeting SARS-CoV-2 spike protein of COVID-19 with naturally occurring phytochemicals: an in silico study for drug development. *J. Biomol. Struct. Dyn.* **2021**, *39*, 6306−6316.
(13) Faheem; Kumar, B. K.; Sekhar, K.; Kunjiappan, S.; Jamalis, J.; Balana-Fouce, R.; Tekwani, B. L.; Sankaranarayanan, M. Druggable targets of SARS-CoV-2 and treatment opportunities for COVID-19. *Bioorg. Chem.* **2020**, *104*, No. 104269.
(14) Wang, M.; Cao, R.; Zhang, L.; Yang, X.; Liu, J.; Xu, M.; Shi, Z.; Hu, Z.; Zhong, W.; Xiao, G. Remdesivir and chloroquine effectively inhibit the recently emerged novel coronavirus (2019-nCoV) in vitro. *Cell Res.* **2020**, *30*, 269−271.
(15) Gao, Y.; Yan, L.; Huang, Y.; Liu, F.; Zhao, Y.; Cao, L.; Wang, T.; Sun, Q.; Ming, Z.; Zhang, L.; Ge, J.; Zheng, L.; Zhang, Y.; Wang, H.; Zhu, Y.; Zhu, C.; Hu, T.; Hua, T.; Zhang, B.; Yang, X.; Li, J.; Yang, H.; Liu, Z.; Xu, W.; Guddat, L. W.; Wang, Q.; Lou, Z.; Rao, Z. Structure of the RNA-dependent RNA polymerase from COVID-19 virus. *Science* **2020**, *368*, 779−782.
(16) Beigel, J. H.; Tomashek, K. M.; Dodd, L. E.; Mehta, A. K.; Zingman, B. S.; Kalil, A. C.; Hohmann, E.; Chu, H. Y.; Luetkemeyer, A.; Kline, S.; Lopez de Castilla, D.; Finberg, R. W.; Dierberg, K.; Tapson, V.; Hsieh, L.; Patterson, T. F.; Paredes, R.; Sweeney, D. A.; Short, W. R.; Touloumi, G.; Lye, D. C.; Ohmagari, N.; Oh, M. D.; Ruiz-Palacios, G. M.; Benfield, T.; Fatkenheuer, G.; Kortepeter, M. G.; Atmar, R. L.; Creech, C. B.; Lundgren, J.; Babiker, A. G.; Pett, S.; Neaton, J. D.; Burgess, T. H.; Bonnett, T.; Green, M.; Makowski, M.; Osinusi, A.; Nayak, S.; Lane, H. C.; Members, A.-S. G. Remdesivir for the Treatment of Covid-19 - Final Report. *N. Engl. J. Med.* **2020**, *383*, 1813−1826.
(17) Cai, Q.; Yang, M.; Liu, D.; Chen, J.; Shu, D.; Xia, J.; Liao, X.; Gu, Y.; Cai, Q.; Yang, Y.; Shen, C.; Li, X.; Peng, L.; Huang, D.; Zhang, J.; Zhang, S.; Wang, F.; Liu, J.; Chen, L.; Chen, S.; Wang, Z.; Zhang, Z.; Cao, R.; Zhong, W.; Liu, Y.; Liu, L. Experimental Treatment with Favipiravir for COVID-19: An Open-Label Control Study. *Engineering (Beijing)* **2020**, *6*, 1192−1198.
(18) Hillen, H. S.; Kokic, G.; Farnung, L.; Dienemann, C.; Tegunov, D.; Cramer, P. Structure of replicating SARS-CoV-2 polymerase. *Nature* **2020**, *584*, 154−156.
(19) Wang, Q.; Wu, J.; Wang, H.; Gao, Y.; Liu, Q.; Mu, A.; Ji, W.; Yan, L.; Zhu, Y.; Zhu, C.; Fang, X.; Yang, X.; Huang, Y.; Gao, H.; Liu, F.; Ge, J.; Sun, Q.; Yang, X.; Xu, W.; Liu, Z.; Yang, H.; Lou, Z.; Jiang, B.; Guddat, L. W.; Gong, P.; Rao, Z. Structural Basis for RNA

Replication by the SARS-CoV-2 Polymerase. *Cell* **2020**, *182*, 417−413.
(20) Simonis, A.; Theobald, S. J.; Fatkenheuer, G.; Rybniker, J.; Malin, J. J. A comparative analysis of remdesivir and other repurposed antivirals against SARS-CoV-2. *EMBO Mol. Med.* **2021**, *13*, No. e13105.
(21) Yin, W.; Mao, C.; Luan, X.; Shen, D. D.; Shen, Q.; Su, H.; Wang, X.; Zhou, F.; Zhao, W.; Gao, M.; Chang, S.; Xie, Y. C.; Tian, G.; Jiang, H. W.; Tao, S. C.; Shen, J.; Jiang, Y.; Jiang, H.; Xu, Y.; Zhang, S.; Zhang, Y.; Xu, H. E. Structural basis for inhibition of the RNA-dependent RNA polymerase from SARS-CoV-2 by remdesivir. *Science* **2020**, *368*, 1499−1504.
(22) Peng, Q.; Peng, R.; Yuan, B.; Zhao, J.; Wang, M.; Wang, X.; Wang, Q.; Sun, Y.; Fan, Z.; Qi, J.; Gao, G. F.; Shi, Y. Structural and biochemical characterization of the nsp12-nsp7-nsp8 core polymerase complex from SARS-CoV-2. *Cell Rep.* **2020**, *31*, 107774−107788.
(23) Jayk Bernal, A.; Gomes Da Silva, M. M.; Musungaie, D. B.; Kovalchuk, E.; Gonzalez, A.; Delos Reyes, V.; Martin-Quiros, A.; Caraco, Y.; Williams-Diaz, A.; Brown, M. L.; Du, J.; Pedley, A.; Assaid, C.; Strizki, J.; Grobler, J. A.; Shamsuddin, H. H.; Tipping, R.; Wan, H.; Paschke, A.; Butterton, J. R.; Johnson, M. G.; De Anda, C.; Group, M. O.-O. S. Molnupiravir for Oral Treatment of Covid-19 in Nonhospitalized Patients. *N. Engl. J. Med.* **2022**, *386*, 509−520.
(24) Lee, C. C.; Hsieh, C. C.; Ko, W. C. Molnupiravir-A Novel Oral Anti-SARS-CoV-2 Agent. *Antibiotics (Basel)* **2021**, *10*, 1294.
(25) Mahase, E. Covid-19: Molnupiravir reduces risk of hospital admission or death by 50% in patients at risk, MSD reports. *BMJ* **2021**, *375*, No. n2422.
(26) Wang, Y.; Li, P.; Solanki, K.; Li, Y.; Ma, Z.; Peppelenbosch, M. P.; Baig, M. S.; Pan, Q. Viral polymerase binding and broad-spectrum antiviral activity of molnupiravir against human seasonal coronaviruses. *Virology* **2021**, *564*, 33−38.
(27) Kabinger, F.; Stiller, C.; Schmitzova, J.; Dienemann, C.; Kokic, G.; Hillen, H. S.; Hobartner, C.; Cramer, P. Mechanism of molnupiravir-induced SARS-CoV-2 mutagenesis. *Nat. Struct. Mol. Biol.* **2021**, *28*, 740−746.
(28) Swanstrom, R.; Schinazi, R. F. Lethal mutagenesis as an antiviral strategy. *Science* **2022**, *375*, 497−498.
(29) Toots, M.; Yoon, J. J.; Hart, M.; Natchus, M. G.; Painter, G. R.; Plemper, R. K. Quantitative efficacy paradigms of the influenza clinical drug candidate EIDD-2801 in the ferret model. *Transl. Res.* **2020**, *218*, 16−28.
(30) Sheahan, T. P.; Sims, A. C.; Zhou, S.; Graham, R. L.; Pruijssers, A. J.; Agostini, M. L.; Leist, S. R.; Schafer, A.; Dinnon, K. H.; Stevens, L. J.; Chappell, J. D.; Lu, X.; Hughes, T. M.; George, A. S.; Hill, C. S.; Montgomery, S. A.; Brown, A. J.; Bluemling, G. R.; Natchus, M. G.; Saindane, M.; Kolykhalov, A. A.; Painter, G.; Harcourt, J.; Tamin, A.; Thornburg, N. J.; Swanstrom, R.; Denison, M. R.; Baric, R. S. An orally bioavailable broad-spectrum antiviral inhibits SARS-CoV-2 in human airway epithelial cell cultures and multiple coronaviruses in mice. *Sci. Transl. Med.* **2020**, *12*, No. eabb5883.
(31) Crotty, S.; Cameron, C. E.; Andino, R. RNA virus error catastrophe: direct molecular test by using ribavirin. *Proc. Natl. Acad. Sci. U. S. A.* **2001**, *98*, 6895−6900.
(32) Urakova, N.; Kuznetsova, V.; Crossman, D. K.; Sokratian, A.; Guthrie, D. B.; Kolykhalov, A. A.; Lockwood, M. A.; Natchus, M. G.; Crowley, M. R.; Painter, G. R.; Frolova, E. I.; Frolov, I. beta-d-N(4)-Hydroxycytidine Is a Potent Anti-alphavirus Compound That Induces a High Level of Mutations in the Viral Genome. *J. Virol.* **2018**, *92*, 10−1128.
(33) Zhao, Y.; Truhlar, D. G. Exploring the limit of accuracy of the global hybrid meta density functional for main-group thermochemistry, kinetics, and noncovalent interactions. *J. Chem. Theory Comput.* **2008**, *4*, 1849−1868.
(34) Ibrahim, M. A. A. Molecular mechanical perspective on halogen bonding. *J. Mol. Model.* **2012**, *18*, 4625−4638.
(35) Boys, S. F.; Bernardi, F. The calculation of small molecular interactions by the differences of separate total energies. Some procedures with reduced errors. *Mol. Phys.* **1970**, *19*, 553−566.
(36) Jeziorski, B.; Moszynski, R.; Szalewicz, K. Perturbation-theory approach to intermolecular potential-energy surfaces of van der Waals complexes. *Chem. Rev.* **1994**, *94*, 1887−1930.
(37) Parrish, R. M.; Burns, L. A.; Smith, D. G. A.; Simmonett, A. C.; DePrince, A. E.; Hohenstein, E. G.; Bozkaya, U.; Sokolov, A. Y.; Di Remigio, R.; Richard, R. M.; Gonthier, J. F.; James, A. M.; McAlexander, H. R.; Kumar, A.; Saitow, M.; Wang, X.; Pritchard, B. P.; Verma, P.; Schaefer, H. F.; Patkowski, K.; King, R. A.; Valeev, E. F.; Evangelista, F. A.; Turney, J. M.; Crawford, T. D.; Sherrill, C. D. Psi4 1.1: An open-source electronic structure program emphasizing automation, advanced libraries, and interoperability. *J. Chem. Theory Comput.* **2017**, *13*, 3185−3197.
(38) Hohenstein, E. G.; Parrish, R. M.; Sherrill, C. D.; Turney, J. M.; Schaefer, H. F. Large-scale symmetry-adapted perturbation theory computations via density fitting and Laplace transformation techniques: investigating the fundamental forces of DNA-intercalator interactions. *J. Chem. Phys.* **2011**, *135*, 174107−174119.
(39) Hohenstein, E. G.; Sherrill, C. D. Density fitting and Cholesky decomposition approximations in symmetry-adapted perturbation theory: Implementation and application to probe the nature of pi-pi interactions in linear acenes. *J. Chem. Phys.* **2010**, *132*, 184111−184120.
(40) Parker, T. M.; Burns, L. A.; Parrish, R. M.; Ryno, A. G.; Sherrill, C. D. Levels of symmetry adapted perturbation theory (SAPT). I. Efficiency and performance for interaction energies. *J. Chem. Phys.* **2014**, *140*, No. 094106.
(41) Lu, T.; Chen, F. Multiwfn: a multifunctional wavefunction analyzer. *J. Comput. Chem.* **2012**, *33*, 580−592.
(42) Humphrey, W.; Dalke, A.; Schulten, K. VMD: Visual molecular dynamics. *J. Mol. Graph.* **1996**, *14*, 33−38.
(43) Tomasi, J.; Mennucci, B.; Cammi, R. Quantum mechanical continuum solvation models. *Chem. Rev.* **2005**, *105*, 2999−3094.
(44) Marenich, A. V.; Cramer, C. J.; Truhlar, D. G. Universal solvation model based on solute electron density and on a continuum model of the solvent defined by the bulk dielectric constant and atomic surface tensions. *J. Phys. Chem. B* **2009**, *113*, 6378−6396.
(45) J., Frisch; Trucks, G. W.; H. B., Schlegel; G. E., Scuseria; M. A., Robb; J. R., Cheeseman; G., Scalmani; V., Barone; B., Mennucci; G. A., Petersson; H., Nakatsuji; M., Caricato; X., Li; H. P., Hratchian; A. F., Izmaylov; J., Bloino; G., Zheng; J. L., Sonnenberg; M., Hada; M., Ehara; K., Toyota; R., Fukuda; J., Hasegawa; M., Ishida; T., Nakajima; Y., Honda; O., Kitao; H., Nakai; T., Vreven; J. A., Montgomery, Jr.; J. E., Peralta; F., Ogliaro; M., Bearpark; J. J., Heyd; E., Brothers; K. N., Kudin; V. N., Staroverov; R., Kobayashi; J., Normand; K., Raghavachari; A., Rendell; J. C., Burant; S. S., Iyengar; J., Tomasi; M., Cossi; N., Rega; J. M., Millam; M., Klene; J. E., Knox; J. B., Cross; V., Bakken; C., Adamo; J., Jaramillo; R., Gomperts; R. E., Stratmann; O., Yazyev; A. J., Austin; R., Cammi; C., Pomelli; J. W., Ochterski; R. L., Martin; K., Morokuma; V. G., Zakrzewski; G. A., Voth; P., Salvador; J. J., Dannenberg; S., Dapprich; A. D., Daniels; Ö., Farkas; J. B., Foresman; J. V., Ortiz; J., Cioslowski; D. J., Fox *Gaussian 09*, Gaussian, Inc.: Wallingford CT, Revision E.01. 2009.
(46) Sharov, A. V.; Burkhanova, T. M.; Taskin Tok, T.; Babashkina, M. G.; Safin, D. A. Computational Analysis of Molnupiravir. *Int. J. Mol. Sci.* **2022**, *23*, 1508.
(47) Murray, J. S.; Politzer, P. The electrostatic potential: An overview. *Wiley Interdiscip. Rev. Comput. Mol. Sci.* **2011**, *1*, 153−163.
(48) Weiner, P. K.; Langridge, R.; Blaney, J. M.; Schaefer, R.; Kollman, P. A. Electrostatic potential molecular surfaces. *Proc. Natl. Acad. Sci. U. S. A.* **1982**, *79*, 3754−3758.
(49) Varadwaj, P. R.; Varadwaj, A.; Marques, H. M. Halogen bonding: A halogen-centered noncovalent interaction yet to be understood. *Inorganics* **2019**, *7*, 40−102.
(50) Contreras-Garcia, J.; Johnson, E. R.; Keinan, S.; Chaudret, R.; Piquemal, J. P.; Beratan, D. N.; Yang, W. NCIPLOT: A program for plotting non-covalent interaction regions. *J. Chem. Theory Comput.* **2011**, *7*, 625−632.
(51) Panini, P.; Gonnade, R. G.; Chopra, D. Experimental and computational analysis of supramolecular motifs involving Csp2-


https://doi.org/10.1021/acsomega.3c03215
*ACS Omega* 2023, 8, 27553−27565

(aromatic)−F and CF3 groups in organic solids. *New J. Chem.* **2016**, *40*, 4981−5001.
(52) Bader, R. F. W. Atoms in molecules. *Acc. Chem. Res.* **1985**, *18*, 9−15.
(53) Gu, Y.; Kar, T.; Scheiner, S. Fundamental Properties of the CH···O Interaction: Is It a True Hydrogen Bond? *J. Am. Chem. Soc.* **1999**, *121*, 9411−9422.



https://doi.org/10.1021/acsomega.3c03215
*ACS Omega* 2023, 8, 27553−27565